J Intell Robot Syst (2017) 88:415–436
DOI 10.1007/s10846-017-0535-4

Active Fault-Tolerant Control of Unmanned Quadrotor Helicopter Using Linear Parameter Varying Technique

Zhixiang Liu · Chi Yuan · Youmin Zhang

Received: 13 September 2016 / Accepted: 8 March 2017 / Published online: 29 March 2017

Abstract By adopting the linear parameter varying (LPV) control technique, this paper presents an active fault-tolerant control (FTC) strategy with application to unmanned quadrotor helicopter (UQH). Adverse effects from payload grasping and dropping caused variations of system dynamics as well as battery drainage induced loss of actuator effectiveness are expected to be counteracted in this study. First, the UQH is manipulated by a well designed baseline controller. In the presence of either payload grasping/dropping or battery drainage, their magnitudes are then obtained from a LPV-based fault detection and diagnosis (FDD) scheme. Next, based on the estimated values, a fault-tolerant tracking controller, which is linear parameter dependent, is devised in a convex polytopic LPV representation schedules to a new status in corresponding to the system variations, so that the negative impacts can be compensated. The parameters that change with system variations are specified as scheduling scalars for the LPV controller, while the ultimate control rule is obtainable by employing a set of well-established linear matrix inequality (LMI) conditions. Finally, both numerical simulations on a nonlinear model of UQH and experiments on a real UQH are conducted so as to testify the effectiveness of proposed methodology.

Keywords Unmanned quadrotor helicopter · Linear parameter varying · Fault detection and diagnosis · Fault-tolerant control · Payload variation · Battery drainage · Linear matrix inequality

1 Introduction

In the past decade, unmanned aerial vehicles (UAVs), which have been increasingly employed by universities, research institutes, commercial entities, and military in their respective applications, are experiencing an unprecedented growth. As an important class of UAV, unmanned quadrotor helicopter (UQH) owns tremendous advantages over other types of aircrafts including fixed-wing and rotary-wing aircrafts [1]. These merits include their decreased mechanical structure complicity [2], relatively affordable cost of development and maintenance [1], easy-to-fly [3], and enhanced maneuverability and deployability [4, 5]. These properties have contributed tremendous benefits to a diversity of

Z. Liu · C. Yuan · Y. Zhang (✉)
Department of Mechanical and Industrial Engineering, Concordia University, 1455 de Maisonneuve Blvd. W., Montreal, QC H3G 1M8, Canada
e-mail: ymzhang@encs.concordia.ca

Z. Liu
e-mail: lzhx180@gmail.com

C. Yuan
e-mail: chiyuan996@gmail.com

Y. Zhang
Shaanxi Key Laboratory of Complex System Control and Intelligent Information Processing, Xi'an University of Technology, Xi'an, Shaanxi 710048, China

practical applications including search and rescue [6], environmental sampling [7], forest fire monitoring, detection and fighting [8], cooperative task accomplishment [9–11], objects recognition [12], as well as military missions [13].

Along these lines, there is also an increasing interest in developing UQHs capable of grasping and dropping payloads suddenly and dramatically for a variety of missions, such as express delivery, fire/oil leaking monitoring and detection with visual/infrared cameras onboard UQHs [8], in-flight replenishment [14], missile launching, environmental sampling, and post-disaster search and rescue including earthquake, hurricane, flood, and other natural disasters [15–17]. Amazon, in particular, has just released its Amazon Prime Air service. This kind of creative and advanced goods delivery technology provides a novel and efficient way to deliver customers' parcels using UQHs within 30 minutes or less. Due to the insufficient collision avoidance capabilities of currently developed UQHs and security concerns of the public, although there is still a long way for UQHs to receive the authorization from the Federal Aviation Administration (FAA) of United States (US) and being extensively and abundantly deployed, much more attention and extensive works have already been dedicated to this promising field. However, it is still challenging for UQHs to appropriately grasp and drop the payloads, this is due to the fact that UQHs are required to stay in balance during flight when payloads are attached to or dropped off the vehicles. Two factors contribute to this phenomenon, the improperly trimmed offset loads and unevenly placed payload may generate the bias forces causing the UQH imbalanced; besides, the added or dropped payload mass may significantly affect the dynamic response of UQH system as well [18]. These factors can ultimately deteriorate the performance of UQHs' controllers that are designed based on the static internal model. More seriously, they may also cause a frequent operation of actuators resulting in the wear and tear of actuators, which can severely reduce the operating lifetime of actuators, lead to the missions being aborted, and probably threaten the safety of personnels, other vehicles, and infrastructures either in their proximity or on the ground [19]. Recent years have seen numerous relevant research activities conducted. Both gain-scheduling PID and model predictive control (MPC) techniques are adopted in [20] for compensating the system variation caused by payload dropping. [21] has introduced an additional mechanism with integration of the conventional proportional-integral-derivative (PID) control to mitigate the system performance deterioration induced by the payload variation. In [22, 23], the cooperative transportation of goods employing a group of UQHs is also studied. Moreover, [18] investigates the stability property of UQH under classical PID control in the presence of added payload mass, but no additional compensating strategy is introduced.

In addition to payload variation issues, as built by various consumable hardwares, UQHs' low development cost may seriously affect their system reliability and safety. Some specific tasks may bring UQHs into sophisticated and hazardous situations as well, such as forest fire monitoring and fighting, and missions execution in rough weather conditions or cluttered mountainous regions. A recent Washington Post investigation reports that more than 400 military UAVs in US have crashed since 2001. Commercial UAV accidents are expected to be far more than that experienced in the military. Although there is no report on civilian casualty due to commercial UAV crashes since 2013, collisions of UAVs with airports, houses, farms, and many other infrastructures have been occasionally reported. Among these accidents, actuator faults, which can cause serious deterioration of system performance and even result in catastrophic consequences (crash), have been realized as one of the predominant adverse factors. In practice, almost all of the existing UQHs are powered by batteries. As a specific type of fault and inevitable phenomenon during the flight of UQHs, the battery voltage generally decreases over time, which is called the battery drainage. The corresponding relationship between the control signal and actual thrust of propeller varies, resulting in a partial loss of control effectiveness of the produced thrusts of propellers. Therefore, the anticipated performance of UQHs cannot be guaranteed. Unfortunately, the enhanced reliability and safety demands are typically far beyond that the classical control approach can offer. The development of more effective and advanced fault-tolerant control (FTC) methodologies [24] thereby deserves further investigations. Despite this, only few of the existing research activities have been carried out on this topic. A multiple subsystems control strategy is presented in [21], the PID control approach is first chosen for designing the baseline controller subsystem, ensuring the desired performance

and system stability; then a battery drainage compensating subsystem is developed to estimate and generate the appropriate control command to mitigate the negative impact of battery drainage induced loss of control effectiveness. [25, 26] have addressed a feedforward neural-network structure for counteracting the power loss in batteries.

Most of the existing UQHs control strategies [27, 28] are developed on the basis of the linearization of nonlinear systems on a specific working point. For the system working on a wider operating region, however, the controller designed on the linearized model may fail to achieve the satisfactory performance. Alternatively, the linear parameter varying (LPV) control method [29], which is capable of effectively solving this kind of challenging nonlinear problems, has progressed steadily into a mature tool recently [30]. As the gain of LPV controller schedules along with the variation of system dynamics, it possesses a prominent advantage over the fixed-gain controllers, which also contributes to a less conservativeness of the controller. Attributing to its capability in guaranteeing system stability and desired performance over an extended region of operating conditions, LPV control technique has been popularly employed by the industrial communities to solve various practical issues [31]. Actually, the first concept of LPV is appeared in [32] which is to analyze the interpolation and realization problems existing in the traditional gain-scheduling control method. In the successive development, a group of methodologies, such as the linear matrix inequality (LMI) [33], set-invariance methods [34], and stable realizations [35], have been gradually developed to facilitate the LPV controller design and enhance its capabilities.

In order to surmount the challenges introduced above, ensure the control effort is sufficient for the operation of low-cost UQH in real-time, and successfully accomplish assigned tasks, as a promising solution, an adaptive LPV reconfigurable parameter estimation and control approach is developed in this research for improving the fault-tolerant capabilities of UQH in the presence of variations in either payload or control effectiveness of actuator. It is expected that these adverse system variations can be effectively adapted with a graceful degradation of system performance [36]. The basic concept behind the presented method is to design a time-varying parameter estimation scheme to capture and a control scheme to accommodate the system variations. This work treats the voltage variation in battery as a kind of loss of control effectiveness fault [37], which is reasonable and practical due to the fact that the thrust of each actuator is proportional to the voltage of battery. This relationship can be interpreted as, with the same control signal, higher voltage indicates more thrust, while lower voltage means less thrust. When the voltage of battery drops, the control effectiveness also changes over time, this phenomenon can then be seen as time-varying state of actuator limited in a specific bound. In addition to that, the variation of payload mass is also selected as the time-varying parameter altering within a certain range. Different from the work suggested in [38], this study tends to develop the fault detection and diagnosis (FDD) [39] and FTC schemes with inclusion of both translational and rotational motions of UQH, which is intended to facilitate the overall control system design. Moreover, a smooth switching mechanism for control gains is likewise designed for the purpose of reducing the side effects of transient phenomenon induced by the abrupt transition between distinctive control laws.

The proposed strategy is constituted by following components: 1) a robust state-feedback controller capable of guaranteeing system stability in the absence of system variations and actuator faults is first designed as the baseline controller; 2) in the event of payload variations or actuator faults, the values of actuator faults can then be diagnosed by an adaptive finite-time LPV-based fault estimation scheme, while the values of payload variations are assumed to be known in practical applications. The variations of payloads and actuator faults are seen as scheduling variables constrained within a constant bound in the LPV scheme design; 3) next, choosing the boundary of these variables as vertices, several sets of control gains are generated offline for each vertex employing the robust state-feedback control scheme which is also designed for the baseline controller; 4) finally, a LPV-based state feedback controller is synthesized to manoeuvre UQH with satisfactory performance in the presence of sudden and dramatic changes in dynamics. The ultimate control gain is calculated in the real-time application based on the estimated values of variables and the control gains obtained in advance for each vertex by adopting the *bounding box approach* introduced in [40]. In order to demonstrate the effectiveness of the proposed approach, extensive simulations on a nonlinear UQH

model and experimental validation on a real UQH are carried out.

The rest of this paper is organized as follows: Section 2 addresses some preliminaries for UQH modelling and control schemes design. Section 3 provides the detailed design procedure of proposed approaches. Section 4 introduces the conducted simulation and experimental validations and analyses the corresponding results. Concluding remarks and future works are summarized in the last section.

For the convenience of readers, throughout this paper, the symbols of UQH model are all defined in Table 1, while the definition of symbols frequently used in the control scheme design are also summarized in Table 2.

2 Preliminaries

Figure 1 shows a typical UQH, which is cooperatively operated by four direct current (DC) motor-driven propellers configured at the front, rear, left, and right corners, respectively. Thrusts u_1, u_2, u_3, and u_4 are generated by these propellers. The front and rear propellers rotate clockwise, while the right and left propellers spin counter-clockwise. The totally created thrusts always direct upward along the z_B-direction. Hence, the vertical translation is performed by straightforwardly distributing identical amount of control signal to each motor, while the horizontal translation is obtained by assigning a distinctive amount of control signals to the opposite motors, so that the UQH can roll/pitch towards the slowest motor, the lateral/forward movement can then be achieved [1].

Table 1 Nomenclature (earth-fixed coordinate system)

Symbols	Explanation
x, y, z	Coordinates of UQH at center of mass
θ	Pitch angle
ϕ	Roll angle
ψ	Yaw angle
$u_z(t)$	Total lift force
$u_\theta(t)$	The applied torque in θ direction
$u_\phi(t)$	The applied torque in ϕ direction
$u_\psi(t)$	The applied torque in ψ direction
K_n $(n = 1, 2, ..., 6)$	Drag coefficients
$u_i(t)$ $(i = 1, 2, 3, 4)$	Thrust of each rotor
L	Center distance between the gravity of UQH and each propeller
C_m	Thrust-to-moment scaling factor
g	Acceleration of gravity
m	UQH mass
I_x	Moment of inertia along x direction
I_y	Moment of inertia along y direction
I_z	Moment of inertia along z direction
ω_m	Actuator bandwidth
K_m	A positive gain
$u_{ci}(t)$ $(i = 1, 2, 3, 4)$	PWM signals distributed to each rotor

Table 2 Nomenclature (symbols for control law design)

Symbols	Explanation
$x(t) \in \Re^n$	State vector
$u(t) \in \Re^m$	Control input
$\delta = [\delta_1, ..., \delta_n]$	A time-varying vector of scheduling variables
$y_{ref}(t)$	The reference command
$u_f(t) = [u_{f1}(t), ..., u_{fm}(t)]^T$	The faulty control input
$L_f = diag\{l_{f1}, ..., l_{fm}\}$	The control effectiveness factors
$\hat{L}_f$	The estimation control effectiveness factors
$K_o(\delta)$	The parameter-varying observer gain
$u(t) = [u_1(t), ..., u_m(t)]^T$	The fault-free control input

2.1 Nonlinear Model of Unmanned Quadrotor Helicopter

As described in [1], a classical UQH dynamic model with respect to the earth-fixed coordinate system can be represented as:

$$\ddot{x} = \frac{(sin\psi sin\phi + cos\psi sin\theta cos\phi)u_z(t) - K_1\dot{x}}{m}$$

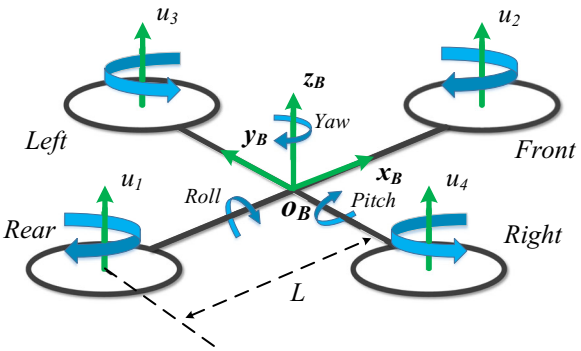

Fig. 1 Schematic diagram of a general UQH

$$\begin{aligned}
\ddot{y} &= \frac{(sin\psi sin\theta cos\phi - cos\psi sin\phi)u_z(t) - K_2\dot{y}}{m} \\
\ddot{z} &= \frac{(cos\theta cos\phi)u_z(t) - K_3\dot{z}}{m} - g \\
\ddot{\phi} &= \frac{u_\phi(t) - K_4\dot{\phi}}{I_x} \\
\ddot{\theta} &= \frac{u_\theta(t) - K_5\dot{\theta}}{I_y} \\
\ddot{\psi} &= \frac{u_\psi(t) - K_6\dot{\psi}}{I_z}.
\end{aligned} \tag{1}$$

The relationship between accelerations and forces is:

$$\begin{bmatrix} u_z(t) \\ u_\theta(t) \\ u_\phi(t) \\ u_\psi(t) \end{bmatrix} = \begin{bmatrix} 1 & 1 & 1 & 1 \\ L & -L & 0 & 0 \\ 0 & 0 & L & -L \\ C_m & C_m & -C_m & -C_m \end{bmatrix} \begin{bmatrix} u_1(t) \\ u_2(t) \\ u_3(t) \\ u_4(t) \end{bmatrix}. \tag{2}$$

Furthermore, the force generated by each propeller and its corresponding pulse width modulation (PWM) signal has the following relationship:

$$u_i(t) = K_m \frac{\omega_m}{s + \omega_m} u_{ci}(t), i = 1, ..., 4. \tag{3}$$

2.2 Model Simplification

In order to facilitate the control design procedure, a further simplified model is normally preferred other than the nonlinear model (1). Before proceeding to the model simplification, the following assumptions are required:

Assumption 1 *It is assumed that the UQH is in hovering condition during the entire flight period* [1]*, which implies* $u_z(t) \approx mg$*. The deflections of pitch and roll motions are so small that* $sin\phi \approx \phi$ *and* $sin\theta \approx \theta$*. There is no yaw motion such that* $\psi = 0$*. UQH moves in low velocity so that the effects from the drag coefficients are insignificant.*

Based on Assumption 1, nonlinear model (1) can be reduced into:

$$\begin{aligned}
\ddot{x} &= \theta g \\
\ddot{y} &= -\phi g \\
\ddot{z} &= u_z(t)/m - g \\
I_x\ddot{\theta} &= u_\theta(t) \\
I_y\ddot{\phi} &= u_\phi(t) \\
I_z\ddot{\psi} &= u_\psi(t).
\end{aligned} \tag{4}$$

As the time constant of DC motor is much smaller than that of UQH [41], (3) can be further simplified to:

$$K_m \frac{\omega_m}{s + \omega_m} \approx K_m. \tag{5}$$

Therefore, combining with (5), (2) can be rewritten as follows:

$$\begin{bmatrix} u_z(t) \\ u_\theta(t) \\ u_\phi(t) \\ u_\psi(t) \end{bmatrix} = \begin{bmatrix} K_m & K_m & K_m & K_m \\ K_mL & -K_mL & 0 & 0 \\ 0 & 0 & K_mL & -K_mL \\ K_mC_m & K_mC_m & -K_mC_m & -K_mC_m \end{bmatrix} U_c, \tag{6}$$

where $U_c = [u_{c1}(t), u_{c2}(t), u_{c3}(t), u_{c4}(t)]^T$.

2.3 Linear Parameter Varying Representation of UQH Model

Written into state-space representation, the combination of (4) and (6) can be written as:

$$\dot{x}(t) = A(\delta)x(t) + B(\delta)u(t) + G(\delta)g, \tag{7}$$

where $A(\delta) \in \Re^{n\times n}$, $B(\delta) \in \Re^{n\times m}$, and $G(\delta) \in \Re^{n\times r}$. $\delta = [\delta_1, ..., \delta_n]$ contains all probable trajectories of system, and $\delta_i(t)$ is limited in $[\underline{\delta}_i, \bar{\delta}_i]$.

This study assumes that the parameter dependence of the constructed LPV system is affine, that is the matrices $A(\delta)$, $B(\delta)$, and $G(\delta)$ affinely lie on δ when it varies over a fixed polytope. One can then obtain the following simplified UQH model:

$$(A(\delta), B(\delta), G(\delta)) = \sum_{i=1}^{N} \mu_i(A_i, B_i, G(i)), \tag{8}$$

where $\sum_{i=1}^{N} \mu_i(A_i, B_i, G(i)) \in Co\{(A_i, B_i) : i = 1, ..., N\}$, and $Co\{\cdot\}$ represents the convex hull, N denotes the number of vertices which is chosen from the piecewise approximation of the UQH nonlinear system, the convex coordinates $\mu_i \in \Omega$ are measurable or can be estimated online, while the convex set Ω owns the following feature:

$$\Omega = \left\{ \mu_i \in \Re^N, \mu_i \geq 0, \sum_{i=1}^{N} \mu_i = 1 \right\}, \tag{9}$$

where μ_i, which represents the function of δ, can be selected referring to the rule addressed in [40].

In order to effectively eliminate the steady-state error, an integral term is incorporated into the controller design as well. The system (7) can then be augmented as follows:

$$\dot{x}_a(t) = A_a(\delta)x_a(t) + B_a(\delta)u(t) + G_a(\delta)\omega_a(t), \quad (10)$$

where $x_a(t) = \left[\left(\int_0^t \varepsilon(\tau)d\tau\right), \ x(t)\right]^T$, $\omega_a(t) = g$, $y_{ref}(t)\Big]^T$, $\varepsilon(t) = y_{ref}(t) - S_r C x(t)$, $C \in \Re^{p\times n}$, $S_r \in \Re^{l\times p}$ is designed for choosing the required system states.

$$A_a(\delta) = \begin{bmatrix} 0 & -S_r C(\delta) \\ 0 & A(\delta) \end{bmatrix} \in \Re^{(l+n)\times(l+n)},$$

$$B_a(\delta) = \begin{bmatrix} 0 \\ B(\delta) \end{bmatrix} \in \Re^{(l+n)\times m}, \quad (11)$$

$$G_a(\delta) = \begin{bmatrix} 0 & I \\ G(\delta) & 0 \end{bmatrix} \in \Re^{(l+n)\times(l+r)}.$$

2.4 Actuator Faults Formulation

Actuator plays a critical role in the operation of UQHs, the desired system performance and stability may be seriously affected when the actuators fail to operate as expected.

Under actuator faults, the control signal can be reformulated as:

$$u_f(t) = L_f u(t), \quad (12)$$

where $l_{fi} = 1$ means the ith actuator in healthy condition, $l_{fi} = 0$ indicates the corresponding actuator suffers a complete failure, while $0 < l_{fi} < 1$ denotes a partial loss of control effectiveness on the ith actuator.

Therefore, the UQH model (10) treating actuator faults as time-varying parameters can be described in the following LPV faulty system:

$$\dot{x}_a(t) = A_a(\delta)x_a(t) + B_a(\delta)L_f u(t) + G_a(\delta)\omega_a(t). \quad (13)$$

3 Linear Parameter Varying Based Fault Estimation and Tolerant Control Scheme Design

In this section, the design procedure of a LPV-based finite-time adaptive fault estimation scheme is first provided. Then, a LPV-based FTC strategy is introduced against variations of system dynamics; the method to synthesize the control laws and the mechanism to reduce the negative impact of transient phenomenon, are both addressed in details as well. The overall design philosophy of the proposed methodologies is outlined in Fig. 2.

3.1 Design of LPV-Based Finite-Time Adaptive Fault Estimation Scheme

3.1.1 LPV-Based Observer Design

Suppose system without actuator faults can be formulated as:

$$\begin{cases} \dot{x}_a(t) = \sum_{i=1}^{N} \mu_i [A_i x_a(t) + B_i u(t)] \\ y_a(t) = \sum_{i=1}^{N} \mu_i C_{ai} x_a(t). \end{cases} \quad (14)$$

Then, system (14) with actuator fault can be represented as:

$$\begin{cases} \dot{x}_a(t) = \sum_{i=1}^{N} \mu_i [A_i x_a(t) + B_a L_{fi}(t) u(t)] \\ y_a(t) = \sum_{i=1}^{N} \mu_i C_{ai} x_a(t). \end{cases} \quad (15)$$

To estimate the effectiveness of each faulty actuator, the following adaptive fault diagnosis observer is constructed:

$$\begin{cases} \dot{\hat{x}}_a(t) = \sum_{i=1}^{N} \mu_i [A_i \hat{x}_a(t) + B_a \hat{L}_{fi}(t) u(t) - K_{oi}(\hat{y}_a(t) - y_a(t))] \\ \hat{y}_a(t) = \sum_{i=1}^{N} \mu_i C_{ai} \hat{x}_a(t), \end{cases} \quad (16)$$

where the pair (A_i, C_{ai}) is assumed to be observable, and the observer gain $K_o(\delta)$ is chosen to guarantee the stability of $(A_a(\delta) - K_o(\delta)C_a)$, which is given by:

$$K_o(\delta) = \sum_{i=1}^{N} \mu_i(\delta) K_{oi} > 0, \ \mu_i(\delta) \geq 0, \sum_{i=1}^{N} \mu_i(\delta) = 1. \quad (17)$$

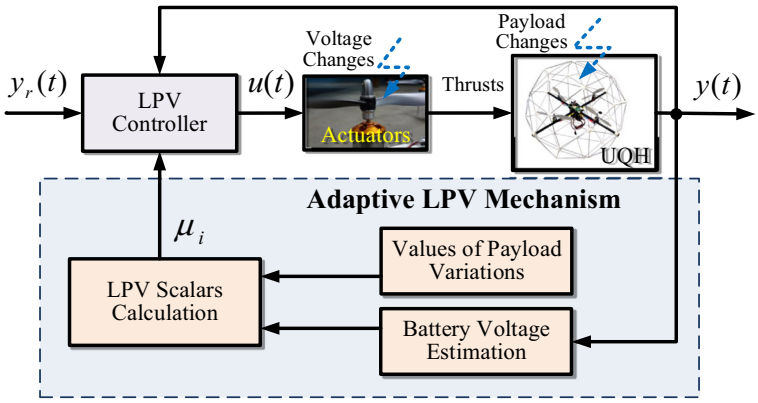

Fig. 2 Schematic illustration of the proposed methods.

Thus, the dynamic error between (15) and (16) can be denoted as:

$$\begin{cases} \dot{e}_x(t) = \sum_{i=1}^{N} \mu_i (A_i - K_{oi} C_{ai}) e_{xi}(t) + B_a e_{fi}(t) u(t) \\ \qquad = \sum_{i=1}^{N} \mu_i [A_{Ki} e_{xi}(t) + B_a e_{fi}(t) u(t)] \\ e_y(t) = \sum_{i=1}^{N} \mu_i C_{ai} e_{xi}(t), \end{cases} \tag{18}$$

where $A_K(\delta) = \sum_{i=1}^{N} \mu_i (A_{Ki})$, and $A_{Ki} = A_i - K_{oi} C_{ai}$. $e_x(t) = \sum_{i=1}^{N} \mu_i e_{xi}(t) = \hat{x}_a(t) - x_a(t)$, $e_y(t) = \sum_{i=1}^{N} \mu_i e_{yi}(t) = \hat{y}_a(t) - y_a(t)$, $e_f(t) = \sum_{i=1}^{N} \mu_i (e_{fi}(t))$, and $e_{fi}(t) = \hat{L}_{fi}(t) - L_{fi}(t)$.

The parameter-varying observer gain $K_o(\delta)$ can then be obtained by the stated LMI conditions in the following proposition.

Proposition 1 *If there exist matrices* $F_i \in \Re^{(n+l)\times(n+l)}$ *and a symmetric matrix* $T \in \Re^{(n+l)\times p}$, *then* $K_{oi} = T_i^{-1} F_i$ *can stabilize* (18) *with the following LMI holds* [42, 43]*:*

$$\begin{bmatrix} T & A_i^T T - C_{ai}^T F_i^T \\ T A_i - F_i C_{ai} & T \end{bmatrix} > 0. \tag{19}$$

Consequently, $K_o(\delta) = \sum_{i=1}^{N} \mu_i (T^{-1} F_i)$.

Proof of Proposition 1 For each vertex, the following Lyapunov function candidate is selected:

$$V_o = e_{xi}^T T e_{xi}. \tag{20}$$

In the absence of actuator faults, the derivative of V_o is:

$$\begin{aligned} \dot{V}_o &= \dot{e}_{xi}^T T e_{xi} + e_{xi}^T T \dot{e}_{xi} \\ &= (A_i - K_{oi} C_{ai})^T T e_{xi}^2 + T (A_i - K_{oi} C_{ai}) e_{xi}^2 \\ &= [(A_i - K_{oi} C_{ai})^T T + T (A_i - K_{oi} C_{ai})] e_{xi}^2. \end{aligned} \tag{21}$$

In order to make $\dot{V}_o < 0$, one can obtain that:

$$(A_i - K_{oi} C_{ai})^T T + T (A_i - K_{oi} C_{ai}) < 0. \tag{22}$$

Choose $K_{oi} = T_i^{-1} F_i$, Eq. 22 becomes:

$$A_i^T T - C_{ai}^T F_i^T + T A_i - F_i C_{ai} < 0. \tag{23}$$

Apply Schur complement [45], Eq. 23 can then be converted to Eq. 19. The proof is completed. □

For the convenience of constructing an adaptive law for the parameter (actuator efficiency factor) estimation, (18) can be rewritten as:

$$\begin{cases} \dot{e}_x(t) = \sum_{i=1}^{N} \mu_i [A_{Ki} e_x(t) + B_a \tilde{L}_f(t) u(t)] \\ e_y(t) = \sum_{i=1}^{N} \mu_i C_{ai} e_x(t), \end{cases} \tag{24}$$

where $\tilde{L}_f(t) = \sum_{i=1}^{N} \mu_i [\hat{L}_{fi}(t) - L_{fi}(t)] = \hat{L}_f(t) - L_f(t)$.

3.1.2 LPV-Based Finite-Time Adaptive Parameter Estimator Design

Defining a regressor matrix $M(t)$, and a vector $N(t)$ as:

$$\begin{cases} \dot{M}(t) = -k_{FF} M(t) + k_{FF} \phi^T(t) \phi(t), \ M(0) = 0 \\ \dot{N}(t) = -k_{FF} N(t) + k_{FF} \phi^T(t) \phi(t) L_f(t), \end{cases} \tag{25}$$

where $k_{FF} \in \Re^+$ denotes a forgetting factor, $\phi(t) = B_a u(t)$, whilst $N(0) = 0$ is the initial condition of $N(t)$.

The solution to (25) can then be obtained:

$$\begin{cases} M(t) = \int_0^t e^{-k_{FF}(t-\tau)} k_{FF} \phi^T(\tau)\phi(\tau) d\tau, \\ N(t) = \int_0^t e^{-k_{FF}(t-\tau)} k_{FF} \phi^T(\tau)\phi(\tau) L_f(t) d\tau \\ \quad\quad = M(t) L_f(t). \end{cases} \tag{26}$$

Therefore, the following equations can be derived:

$$\begin{cases} \tilde{N}(t) = \hat{N}(t) - N(t) = M(t) L_f(t), \\ L_f(t) = M^{-1}(t)\tilde{N}(t). \end{cases} \tag{27}$$

Theorem 1 *The adaptive law can be formulated as:*

$$\dot{\hat{L}}_f(t) = -\Gamma \sum_{i=1}^{N} \mu_i [B_a^T P_i e_x(t) + R(t)], \tag{28}$$

where $R(t)$ is a sliding mode term, which is expected to guarantee the fast parameter convergence and can be written as:

$$\begin{aligned} R(t) &= M(t)\Omega_{f1} \frac{M(t)\hat{L}_f(t) - N(t)}{||M(t)\hat{L}_f(t) - N(t)||} \\ &\quad + M(t)\Omega_{f2}[M(t)\hat{L}_f(t) - N(t)] \\ &= M(t)\Omega_{f1} \frac{\tilde{N}(t)}{||\tilde{N}(t)||} + M(t)\Omega_{f2}\tilde{N}(t), \end{aligned} \tag{29}$$

where $\Omega_{f1} = \omega_{f1}\Omega$ and $\Omega_{f2} = \omega_{f2}\Omega$. ω_{f1} and ω_{f2} are positive definite scalars. $\Omega = diag(\omega_1, \omega_2, ..., \omega_n)$ is a positive definite matrix, and $\Gamma = diag(\tau_1, \tau_2, ..., \tau_n)$ is a learning rate symmetric positive definite matrix.

Proof of Theorem 1 This proof procedure can be divided into two steps:

1. Proving $e_x(t)$ can exponentially decay; and
2. Proving the finite-time convergence property of control input.

Step 1: Choosing the following Lyapunov candidate:

$$\begin{aligned} V &= \frac{1}{2} e_x^T(t) P(\delta) e_x(t) + \frac{1}{2}\tilde{N}^T(t) M^{-1}(t)\Gamma^{-1} M^{-1}(t)\tilde{N}(t) \\ &= \frac{1}{2}\sum_{i=1}^{N} \mu_i \left[e_x^T(t) P_i e_x(t) + \frac{1}{2}\tilde{N}^T(t) M^{-1}(t)\Gamma^{-1} M^{-1}(t)\tilde{N}(t) \right] \\ &> 0, \end{aligned} \tag{30}$$

besides, setting:

$$\begin{aligned} V &= V_1 + V_2, \\ V_1 &= \frac{1}{2}\sum_{i=1}^{N} \mu_i \left[e_x^T(t) P_i e_x(t) \right], \\ V_2 &= \frac{1}{2}\sum_{i=1}^{N} \mu_i \left[\tilde{N}^T(t) M^{-1}(t)\Gamma^{-1} M^{-1}(t)\tilde{N}(t) \right]. \end{aligned} \tag{31}$$

Differentiating (30) with respect to time and applying (24), one can then obtain that:

$$\begin{aligned} \dot{V} &= \frac{1}{2}\sum_{i=1}^{N} \mu_i \left\{ \left[\dot{e}_x^T(t) P_i e_x(t) + e_x^T(t) P_i \dot{e}_x(t) \right] \right. \\ &\quad \left. + \frac{d}{dt}\left[\frac{1}{2}\tilde{N}^T(t) M^{-1}(t)\Gamma^{-1} M^{-1}(t)\tilde{N}(t) \right] \right\} \\ &= \frac{1}{2}\sum_{i=1}^{N} \mu_i \left\{ e_x^T \left[A_{Ki}^T P_i + P_i A_{Ki} \right] e_x + e_x^T P_i B_a \tilde{L}_f(t) \right. \\ &\quad \left. + \tilde{N}^T(t) M^{-1}(t)\Gamma^{-1} \frac{d[M^{-1}(t)\tilde{N}(t)]}{dt} \right\}. \end{aligned} \tag{32}$$

Since $A_K(\delta) = \sum_{i=1}^{N} \mu_i (A_{Ki})$ is a Hurwitz matrix along with the linear varying parameters, the following inequality holds:

$$A_K(\delta)^T P(\delta) + P(\delta) A_K(\delta) = \sum_{i=1}^{N} \mu_i \left[A_{Ki}^T P_i + P_i A_{Ki} \right] \le -Q(\delta), \tag{33}$$

with positive definite matrices $P(\delta) = P^T(\delta) = \sum_{i=1}^{N} \mu_i P_i \in \Re^{(l+n)\times(l+n)}$ and $Q(\delta) = Q^T(\delta) = \sum_{i=1}^{N} \mu_i Q_i \in \Re^{(l+n)\times(l+n)}$.

Successively applying (27), (28), (29) and (33), then (32) can be rewritten as:

$$\begin{aligned} \dot{V} &\le -\frac{1}{2} e_x^T Q(\delta) e_x - \tilde{N}^T(t) M^{-1}(t) R(t) \\ &\le -\frac{1}{2} e_x^T Q(\delta) e_x - \tilde{N}^T(t)\Omega_{f1} \frac{\tilde{N}(t)}{||\tilde{N}(t)||} \\ &\quad - \tilde{N}^T(t)\Omega_{f2}\tilde{N}(t). \end{aligned} \tag{34}$$

For the convenience of plain demonstration, the analysis of each term in (34) is separately conducted as follows:

$$\begin{aligned} -\frac{1}{2} e_x^T Q(\delta) e_x &\le -\frac{1}{2}\frac{\lambda_{min}(Q(\delta))}{\lambda_{max}(P(\delta))} V_1, \\ -\tilde{N}^T(t)\Omega_{f1}\frac{\tilde{N}(t)}{||\tilde{N}(t)||} &\le -\frac{\lambda_{min}(\Omega_{f1})}{\lambda_{max}(\Gamma^{-1/2})\lambda_{max}(M^{-1}(t))} V_2^{1/2}, \\ -\tilde{N}^T(t)\Omega_{f2}\tilde{N}(t) &\le -\frac{\lambda_{min}(\Omega_{f2})}{\lambda_{max}(M^{-1}(t))\lambda_{max}(\Gamma^{-1})\lambda_{max}(M^{-1}(t))} V_2, \end{aligned} \tag{35}$$

where $\lambda_{max}(\cdot)$ and $\lambda_{min}(\cdot)$ represent the maximum and minimum eigenvalues of a specific matrix, respectively.

Therefore, the derivative of the chosen Lyapunov candidate (30) is:

$$\dot{V} \leq -\alpha_1 V_1 - \alpha_2 V_2^{1/2} - \alpha_3 V_2, \tag{36}$$

and $e_x(t)$ can exponentially decay with the existence of $\alpha_1 = \frac{1}{2}\frac{\lambda_{min}(Q(\delta))}{\lambda_{max}(P(\delta))} > 0$, $\alpha_2 = \frac{\lambda_{min}(\Omega_{f1})}{\lambda_{max}(\Gamma^{-1/2})\lambda_{max}(M^{-1}(t))} > 0$, and $\alpha_3 = \frac{\lambda_{min}(\Omega_{f2})}{\lambda_{max}(M^{-1}(t))\lambda_{max}(\Gamma^{-1})\lambda_{max}(M^{-1}(t))} > 0$.

Step 2: Apply (28) and (29), the derivative of V_2 can then be achieved:

$$\begin{aligned}\dot{V}_2 &= -\sum_{i=1}^{N}\mu_i\left[\tilde{N}^T(t)M^{-1}(t)\Gamma^{-1}\Gamma\left(B_a^T P_i e_x(t) + R(t)\right)\right] \\ &= -\sum_{i=1}^{N}\mu_i\left[\tilde{L}_f^T(B_a^T P_i e_x(t)) + \tilde{L}_f^T\left(M(t)\Omega_{f1}\frac{M(t)\tilde{L}_f}{||M(t)\tilde{L}_f||}\right.\right. \\ &\quad \left.\left. + M(t)\Omega_{f2}M(t)\tilde{L}_f\right)\right].\end{aligned} \tag{37}$$

Furthermore, when (35) is applied, (37) can be further derived as:

$$\begin{aligned}\dot{V}_2 &\leq \lambda_{max}\left(\sum_{i=1}^{N}\mu_i P_i\right)||B_a||||e_x||||\tilde{L}_f|| - \lambda_{min}(M)\lambda_{min}(\Omega_{f1})||\tilde{L}_f|| \\ &\quad - \frac{\lambda_{min}(\Omega_{f2})\tilde{N}^2 M^{-1}\Gamma^{-1}M^{-1}}{\lambda_{max}(M^{-1})\lambda_{max}(\Gamma^{-1})\lambda_{max}(M^{-1})} \\ &\leq \frac{-2\left[\lambda_{min}(M)\lambda_{min}(\Omega_{f1}) - \lambda_{max}\left(\sum_{i=1}^{N}\mu_i P_i\right)||B_a||||e_x||\right]V_2^{1/2}}{\lambda_{max}(\Gamma^{-1/2})} \\ &\quad - \alpha_3 V_2 \\ &= -\alpha_e V_2^{1/2} - \alpha_3 V_2,\end{aligned} \tag{38}$$

where $\alpha_e = \frac{2}{\lambda_{max}(\Gamma^{-1/2})}[\lambda_{min}(M)\lambda_{min}(\Omega_{f1}) - \lambda_{max}(\sum_{i=1}^{N}\mu_i P_i)||B_a||||e_x||]$.

Since $||B_a||$ is bounded and $e_x(t) \to 0$, there exists a time interval T_1 so that the following inequality holds for $t > T_1$:

$$\lambda_{min}(M)\lambda_{min}(\Omega_{f1}) > \lambda_{max}\left(\sum_{i=1}^{N}\mu_i P_i\right)||B_a||||e_x||. \tag{39}$$

Consequently, there exists a time threshold T_2 such that $\dot{V}_2 \leq -\alpha_e V_2^{1/2} - \alpha_3 V_2 \leq -\alpha_e V_2^{1/2}$.

Based on the finite-time stability theorem in [44], the finite-time convergence of $\lim_{t\to T_2}\tilde{L}_f = 0$ can thereby be achieved. □

3.2 Design of LPV-Based Fault-Tolerant Control Scheme

The general design procedure of the LPV-based FTC scheme can be summarized as follows:

1. A robust state-feedback controller is designed for operating UQH in different working conditions. The variations of payloads and actuator faults are seen as scheduling variables constrained within their individual bound, these boundaries are selected as vertices. Several sets of control gains are generated offline for each vertex.
2. Then, based on the estimated results, the weighting indexes are achievable by calculating the distance from the current working state of UQH to each neighbouring vertex.
3. Finally, a LPV-based state feedback controller can be synthesized by the calculation of all weighting indexes and their corresponding control gains for all vertices to control UQH with satisfactory performance in the presence of sudden and dramatic changes in dynamics.

3.2.1 Fault-Tolerant Control Scheme Design

It is assumed that the states of the closed-loop system are measurable by the sensors or observable at any time instant. Hence, the augmented system (10) with closed-loop state feedback and the integral tracking action can be written into:

$$u(t) = K_{st}(\delta)x(t) = K_{\varepsilon}(\delta)\int_0^t \varepsilon(\tau)d\tau + K_x(\delta)x(t), \tag{40}$$

where $K_{st}(\delta) = [K_{\varepsilon}(\delta), K_x(\delta)] \in \Re^{m\times(l+n)}$. The corresponding closed-loop augmented system in state feedback case can therein be represented by:

$$\dot{x}_a(t) = A_{st}(\delta)x_a(t) + G_a(\delta)\omega_a(t), \tag{41}$$

where $A_{st}(\delta) = A_a(\delta) + B_a(\delta)K_{st}(\delta)$, and $G_z(\delta) \in \Re^{p\times r}$.

In order to guarantee the existence of the linear parameter dependent state feedback control law (40)

for the closed-loop system (41), the following *bounded real lemma* (BRL) [40] should be satisfied:

1. $A_{st}(\delta)$ is quadratically stable [45];
2. There exists a bound $\gamma > 0$ for any exogenous $\omega_a(t) \in L_2[0.\infty)$, the performance criteria $||T(\delta)||_\infty < \gamma$, where $T(\delta)$ denotes the system transfer function.

If the aforementioned BRL is satisfied, and there exist a symmetric positive definite matrix $X(\delta)$ and a matrix $Y(\delta)$ such that LMI (42) holds [46]:

$$\Xi(\delta)=\begin{bmatrix} A_{lpv}(\delta) & G_a(\delta) & Y^T(\delta)R^{1/2} & X(\delta)Q^{1/2} \\ -\gamma I & * & 0 & 0 \\ * & * & -I & 0 \\ * & * & * & -I \end{bmatrix} < 0, \tag{42}$$

where $A_{lpv}(\delta) = A_a(\delta)X(\delta) + B_a(\delta)Y(\delta) + (A_a(\delta)X(\delta) + B_a(\delta)Y(\delta))^T$.

Remark 1 For the sake of minimizing the conservatism, matrices $X(\delta)$ and $Y(\delta)$ are normally parameterized. However, the nonlinear uncertainty terms may be yielded by the products between the uncertain matrices $A_a(\delta)$ and $X(\delta)$, or $B_a(\delta)$ and $Y(\delta)$. Therefore, the following procedure should be conducted to avoid the nonlinear uncertainty terms by eliminating the elements with the products of two uncertainty terms.

Theorem 2 *The closed-loop system* (41) *can be stabilized under the supervision of state feedback control law* $u(t) = K_{st}(\delta)x_a(t)$ *with* $K_{st}(\delta) = Y(\delta)X^{-1}(\delta)$, *where the positive symmetric matrix* $X(\delta) = \sum_{i=1}^{N}\mu_i X_i \in \Re^{(n+l)\times(n+l)}$ *and matrices* $Y(\delta) = \sum_{i=1}^{N}\mu_i Y_i \in \Re^{n\times(m+l)}$, *if* (43) *and* (44) *hold* (∗ *denotes the symmetric entry in the LMI).*

$$\Xi_{ij} + \Xi_{ji} < 0, \quad (1 \le i \le j \le N), \tag{43}$$

$$\Xi_{ij}=\begin{bmatrix} A_{aj}X_i + B_{aj}Y_i + (A_{aj}X_i + B_{aj}Y_i)^T & G_{aj} & Y_i^T R^{1/2} & X_i Q^{1/2} \\ * & -\gamma I & 0 & 0 \\ * & * & -I & 0 \\ * & * & * & -I \end{bmatrix} < 0. \tag{44}$$

Proof Expanding and parametrizing all terms in (42), then the following sufficient condition of (42) holds:

$$\Xi(\delta) = \sum_{i=1}^{N}\sum_{j=1}^{N}\mu_i\mu_j\Xi_{ij} < 0, \tag{45}$$

where Ξ_{ij} is the same as (43) and (44).

If (43) is true, the following inequalities can thereby be obtained

$$\begin{cases} \Xi_{ii} < 0, & (i = 1, ..., N) \\ \Xi_{ij} + \Xi_{ji} < 0, & (1 \le i < j \le N). \end{cases} \tag{46}$$

As $\sum_{i=1}^{N}\mu_i = 1, \mu_i \ge 0$, then

$$\Xi(\delta) = \sum_{i=1}^{N}\mu_i^2\Xi_{ii} + \sum_{i=1}^{N-1}\sum_{j=i+1}^{N}\mu_i\mu_j\Xi_{ij} < 0, \tag{47}$$

which is equivalent to (45).

Consequently, if (43) holds, it can then derive that (47) is satisfied and (44) holds. Whilst the closed-loop system (41) can be stabilized with respect to all parameter variations δ. □

3.2.2 Control Schemes Synthesis

Employing the *bounding box* method introduced in [40], the LPV system matrices can be approximately described in an affine LPV form [47] as:

$$\begin{cases} A_a(\delta) = A_{a0} + \sum_{i=1}^{N}\mu_i(\delta)A_{ai} \\ B_a(\delta) = B_{a0} + \sum_{i=1}^{N}\mu_i(\delta)B_{ai}, \end{cases} \tag{48}$$

where N is the selected number of vertex.

According to the affine LPV assumption, infinite sets of LMI of (44) can then be reduced to finite evaluation in each vertex of convex set Ω. Thus, the controller for each vertex can be computed offline as $K_i = Y_i X_i^{-1}$ $(i = 1, 2, ..., N)$ [48].

Based on these vertex controllers, the LPV state feedback control law $K_{st}(\delta)$ can ultimately be obtained online as:

$$K_{st}(\delta) = \sum_{i=1}^{N} \mu_i(\delta) K_i, \tag{49}$$

where δ can be measured or estimated in real time, then μ_i can be obtained through $\delta = \sum_{i=1}^{N} \mu_i \delta_i$, and δ_i denotes the value of each vertex.

3.2.3 Reduction of Transient Phenomenon

The switching between two controllers may cause severe transients due to output mismatches of respective controllers. Instead of improving system performance, this phenomenon may seriously degrade system performance and even destabilize system. In order to reduce the negative effects of this phenomenon as much as possible, it is important to remarkably minimize the output mismatches at the instant of switching.

In this study, a smooth switching function, which is intended to guarantee a gentle transition of control laws from fault-free case ($K_{st}(t_0)$) to faulty case (K_f), is designed as follows:

$$K_{st}(t) = K_f + [K_{st}(t_0) - K_f] e^{-\tau(t-t_0)}, \tag{50}$$

where K_{st} denotes the ultimate control gain of the reconfigurable controller, K_f is the control gain under actuator faults, $K_{st}(t_0)$ represents the control gain in the absence of actuator faults, τ is selected based on the performance standard and system dynamics. The design of this function is intended to guarantee a smooth transition from normal case ($K_{st}(t_0)$) to fault-tolerant case (K_f).

4 Results of Simulation and Experiment

In this section, both simulation and experimental implementations of the proposed LPV-based FDD and FTC algorithms are presented. The performance of the proposed LPV-based FTC algorithm, in the presence of actuator faults and mass variations, is compared with a baseline control method. In the simulation, the nonlinear model with Eqs. 1, 2 and 3 is employed for the effectiveness validation of proposed method. While the following linearized model is used for controller design:

$$A = \begin{bmatrix}
0&1&0&0&0&0&0&0&0&0&0&0\\
0&0&0&0&0&0&g&0&0&0&0&0\\
0&0&0&1&0&0&0&0&0&0&0&0\\
0&0&0&0&0&0&0&0&-g&0&0&0\\
0&0&0&0&0&1&0&0&0&0&0&0\\
0&0&0&0&0&0&0&0&0&0&0&0\\
0&0&0&0&0&0&0&1&0&0&0&0\\
0&0&0&0&0&0&0&0&0&0&0&0\\
0&0&0&0&0&0&0&0&0&1&0&0\\
0&0&0&0&0&0&0&0&0&0&0&0\\
0&0&0&0&0&0&0&0&0&0&0&1\\
0&0&0&0&0&0&0&0&0&0&0&0
\end{bmatrix},$$

$$B = \begin{bmatrix}
0&0&0&0\\
0&0&0&0\\
0&0&0&0\\
0&0&0&0\\
0&0&0&0\\
K_m/m&K_m/m&K_m/m&K_m/m\\
0&0&0&0\\
K_mL/I_x&-K_mL/I_x&0&0\\
0&0&0&0\\
0&0&K_mL/I_y&-K_mL/I_y\\
0&0&0&0\\
K_mC/I_z&K_mC/I_z&-K_mC/I_z&-K_mC/I_z
\end{bmatrix},$$

$$C = \begin{bmatrix}
1&0&0&0&0&0&0&0&0&0&0&0\\
0&0&1&0&0&0&0&0&0&0&0&0\\
0&0&0&0&1&0&0&0&0&0&0&0\\
0&0&0&0&0&0&1&0&0&0&0&0
\end{bmatrix},$$

$$G = \begin{bmatrix}0&0&0&0&0&-1&0&0&0&0&0&0\end{bmatrix}^T.$$

System state $x(t) = [x, \dot{x}, y, \dot{y}, z\dot{z}, \phi, \dot{\phi}, \theta, \dot{\theta}, \psi, \dot{\psi}]^T$, control inputs (PWM signals) $u(t) = [u_{c1}, u_{c2}, u_{c3}, u_{c4}]^T$ are all constrained in [0, 0.05].

4.1 Description of Scenarios

In order to achieve a clear and effective evaluation of the proposed algorithms, the following three scenarios are selected:

1. *Scenario 1*: In the first scenario, a loss of 30% control effectiveness, which occurs at 12th second, is injected in two neighbouring (rear and right) motors. This leads to $L_f = diag\{0.7\ 0.7\ 1\ 1\}$.

   The weighting functions $\mu_{ai}(\delta)$ are defined in the following by employing the *bounding box approach* in [40]:

$$\begin{aligned}\mu_{a1}(\delta) &= \frac{\delta_i^1 - \delta_{min}^1}{\delta_{max}^1 - \delta_{min}^1} \\ \mu_{a2}(\delta) &= \frac{\delta_{max}^1 - \delta_i^1}{\delta_{max}^1 - \delta_{min}^1},\end{aligned} \tag{51}$$

   where $\delta_{max}^1 = 1$ and $\delta_{min}^1 = 0.4$ denote the maximum and minimum values of control effectiveness, respectively. The remaining control effectiveness $\delta_i^1 = 0.7$ is defined accordingly. It is noteworthy that the lower bound of δ_i corresponds to the system with actuators all in healthy condition, while the upper bound of δ_i is selected for the acceptable system stability the controller can afford in the occurrence of severest actuator faults.

Table 3 Values of involved system parameters

Parameter	Value	Unit
ω_m	15	rad/s
K_m	120	N
m	1.4	kg
C	1	–
L	0.25	m
I_x	0.03	$kg \cdot m^2$
I_y	0.03	$kg \cdot m^2$
I_z	0.04	$kg \cdot m^2$

In this scenario, the state-feedback control gains for the baseline controller (K_b) and the proposed controller designed for the lower vertices (K_{min}^1) are the same:

$$K_b = K_{min}^1 = \begin{bmatrix} 0 & 0 & 4.4721 & 0 & & \\ 0.0224 & 0 & 0 & 0 & & \\ 0 & -0.0224 & 0 & 0 & & \\ 0 & 0 & 0 & 0.0224 & & \\ 0 & 0 & 0 & 0 & -8.9460 & -6.7118 \\ -0.0616 & -0.0736 & 0 & 0 & 0 & 0 \\ 0 & 0 & 0.0616 & 0.0736 & 0 & 0 \\ 0 & 0 & 0 & 0 & 0 & 0 \\ 0 & 0 & 0 & 0 & 0 & 0 \\ -0.4516 & -0.1661 & 0 & 0 & 0 & 0 \\ 0 & 0 & -0.4516 & -0.1661 & 0 & 0 \\ 0 & 0 & 0 & 0 & -0.0616 & -0.0737 \end{bmatrix}.$$

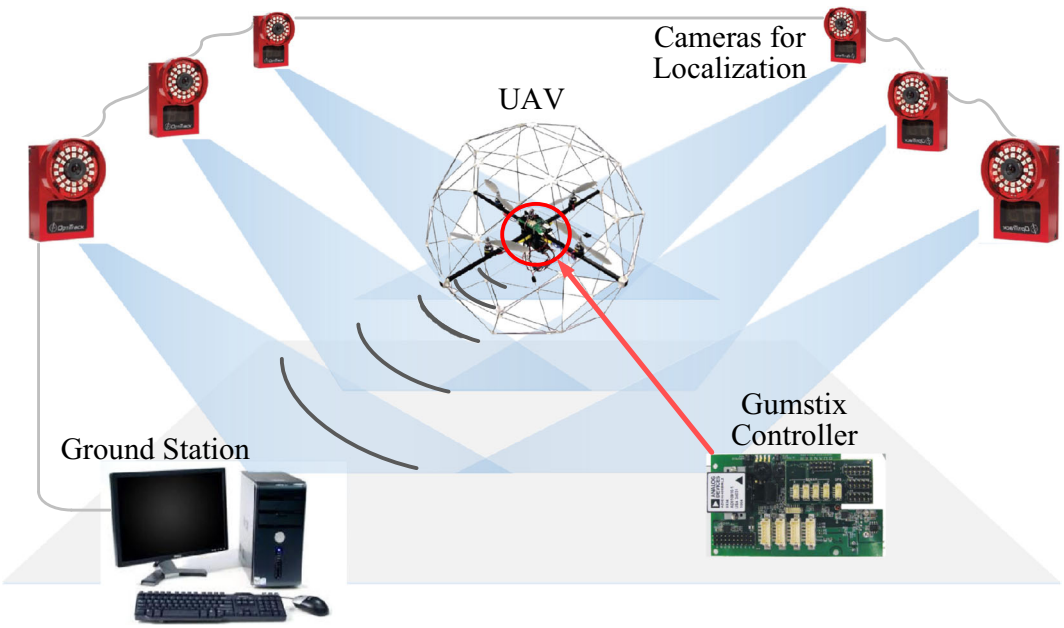

Fig. 3 Layout of the indoor experimental test platform

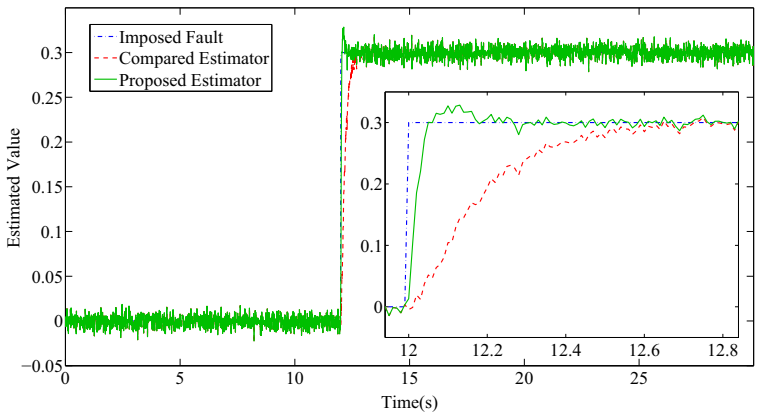

Fig. 4 Performance comparison of fault estimation for the rear motor

The control gain for the baseline controller is kept as the same in the presence/absence of faults, while the proposed controller changes its gain accordingly in regard to the variation of faults. The control gain for the proposed controller is selected as:

$$K_{st1} = \mu_{a1}(\delta)K^1_{min} + \mu_{a2}(\delta)K^1_{max}, \tag{52}$$

where

$$K^1_{max} = \begin{bmatrix} 0 & 0 & 19.9996 & 0 & 0 \\ 0.1000 & 0 & 0 & 0 & -0.2401 \\ 0 & -0.1000 & 0 & 0 & 0 \\ 0 & 0 & 0 & 0.1000 & 0 \\ 0 & 0 & 0 & -35.9869 & -22.3773 \\ -0.2382 & 0 & 0 & 0 & 0 \\ 0 & 0.2401 & 0.2382 & 0 & 0 \\ 0 & 0 & 0 & 0 & 0 \\ 0 & 0 & 0 & 0 & 0 \\ -0.2721 & 0 & 0 & 0 & 0 \\ 0 & -1.0674 & -0.2721 & 0 & 0 \\ 0 & 0 & 0 & -0.2063 & -0.1628 \end{bmatrix}.$$

In this scenario, the weighting functions $\mu_{o1} = 1$ and $\mu_{o2} = 0$ are defined for the proposed adaptive finite-time LPV-based FDD law. Since no payload variation happens, the presented LPV-based FDD law turns to be the finite-time linear time invariant (LTI) FDD law, the gain of which is selected as:

$$K_o = \mu_{o1}(\delta)K_{o1} + \mu_{o2}(\delta)K_{o2}, \tag{53}$$

where K_{o1} and K_{o2} corresponds to the FDD law designed with no and maximum payload variations, respectively.

The performance of the proposed FDD algorithm, in this scenario, is compared with the LTI FDD law in Eq. 28 without sliding mode term.

2. *Scenario 2*: This scenario of simulation considers a loss of 30% control effectiveness imposed in all motors ($L_f = diag\{0.7\ 0.7\ 0.7\ 0.7\}$) and a drop-off of $0.2kg$ payload at 12th second. These actions are expected to cause a transient loss of altitude when the UQH is in hovering condition.

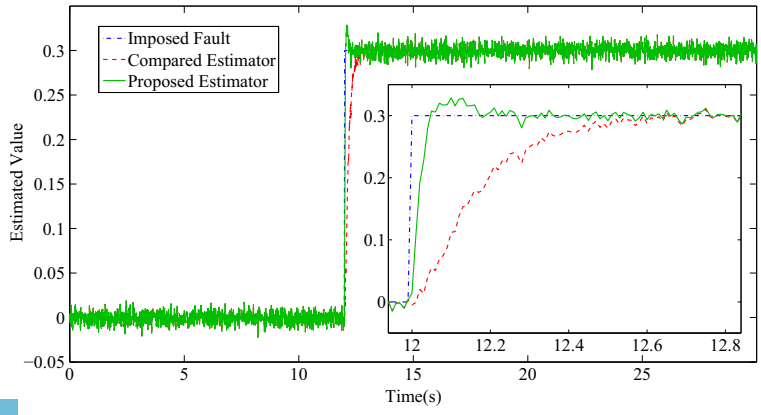

Fig. 5 Performance comparison of fault estimation for the right motor

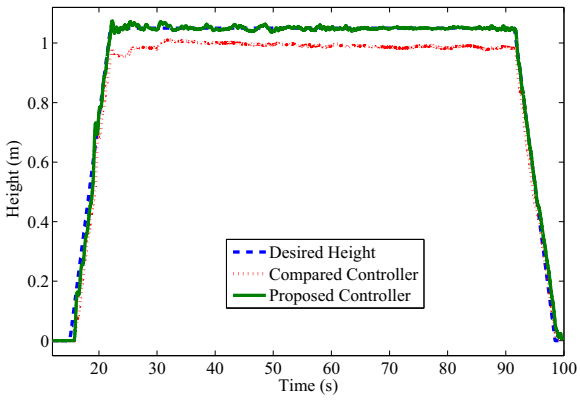

Fig. 6 Performance comparison in vertical direction

Similar to Scenario 1, the weighting functions $\mu_{bi}(\delta)$ in this scenario are chosen as follows:

$$\begin{aligned}
\mu_{b1}(\delta) &= \frac{(\delta_i^A - \delta_{min}^A)}{(\delta_{max}^A - \delta_{min}^A)} \frac{(\delta_i^B - \delta_{min}^B)}{(\delta_{max}^B - \delta_{min}^B)} \\
\mu_{b2}(\delta) &= \frac{(\delta_i^A - \delta_{min}^A)}{(\delta_{max}^A - \delta_{min}^A)} \frac{(\delta_{max}^B - \delta_i^B)}{(\delta_{max}^B - \delta_{min}^B)} \\
\mu_{b3}(\delta) &= \frac{(\delta_{max}^A - \delta_i^A)}{(\delta_{max}^A - \delta_{min}^A)} \frac{(\delta_i^B - \delta_{min}^B)}{(\delta_{max}^B - \delta_{min}^B)} \\
\mu_{b4}(\delta) &= \frac{(\delta_{max}^A - \delta_i^A)}{(\delta_{max}^A - \delta_{min}^A)} \frac{(\delta_{max}^B - \delta_i^B)}{(\delta_{max}^B - \delta_{min}^B)},
\end{aligned} \tag{54}$$

where $\delta_i^A = 1.6$ and $\delta_i^B = 0.7$ denote the time-varying parameters of mass variations and control effectiveness, respectively, while $\delta_{max}^A = 1.8$, $\delta_{max}^B = 1$, $\delta_{min}^A = 1.4$ and $\delta_{min}^B = 0.4$ denote

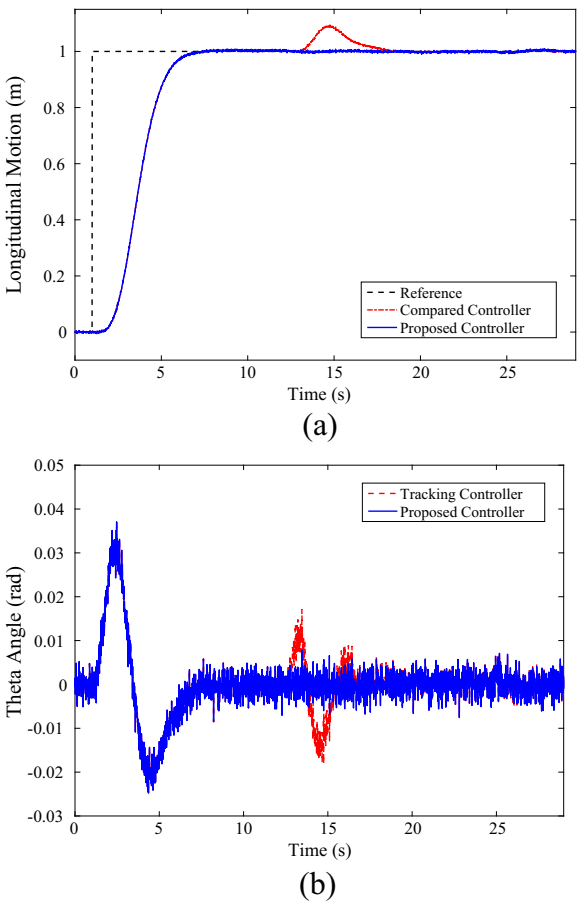

Fig. 7 Performance comparison in longitudinal direction (**a**) and pitch angles (**b**)

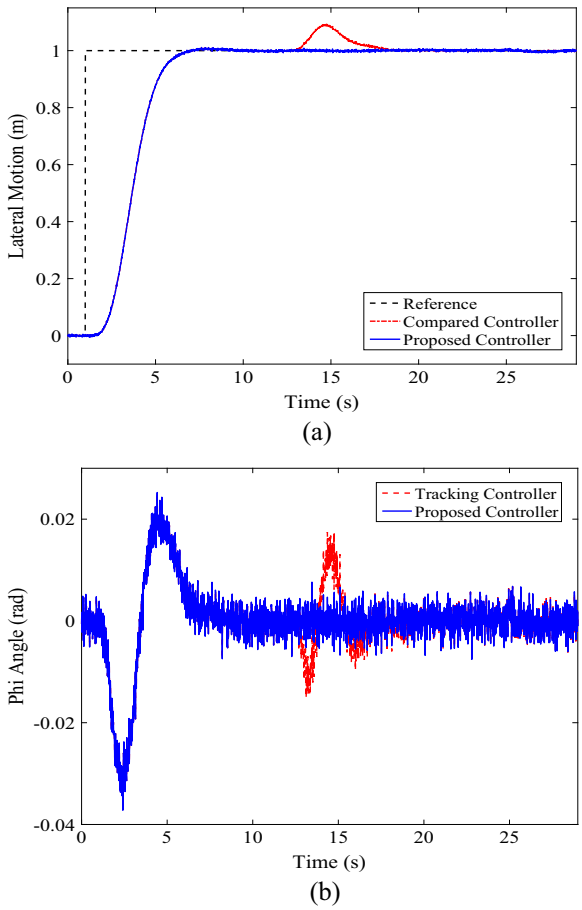

Fig. 8 Performance comparison in lateral direction (**a**) and roll angles (**b**)

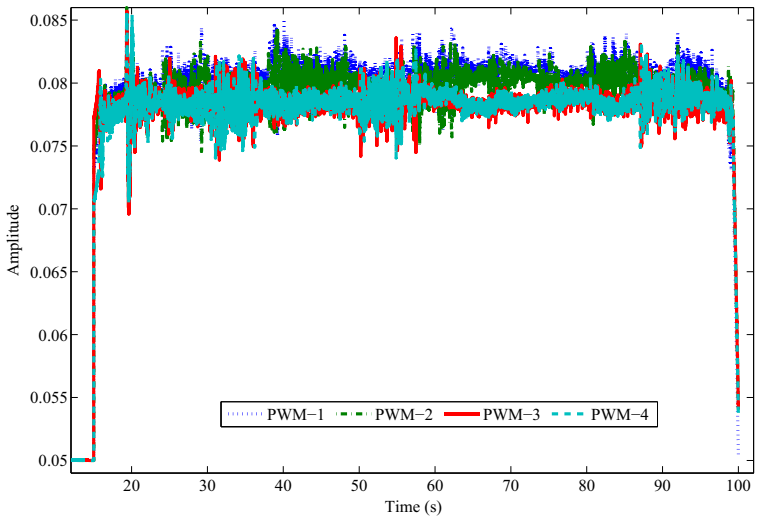

Fig. 9 Performance comparison of PWM signals

the maximum and minimum mass variations and control effectiveness values, respectively.

This scenario chooses the control gain for the baseline controller K_b the same as in Scenario 1, while the control gain for the proposed controller is selected by:

$$K_{st2} = \mu_{b1}(\delta)K_{Bmin}^{Amin} + \mu_{b2}(\delta)K_{Bmax}^{Amin} + \mu_{b3}(\delta)K_{Bmin}^{Amax} + \mu_{b4}(\delta)K_{Bmax}^{Amax}, \quad (55)$$

where K_{Bmin}^{Amin}, K_{Bmax}^{Amin}, K_{Bmin}^{Amax}, and K_{Bmax}^{Amax} represent control gains for the situations of minimum mass variation and control effectiveness, minimum mass variation and maximum control effectiveness, maximum mass variation and minimum control effectiveness, as well as maximum mass variation and maximum control effectiveness, respectively.

The weighting functions $\mu_{oi}(\delta)$ chosen for the proposed adaptive finite-time LPV-based FDD law are defined as follows:

$$\mu_{o1}(\delta) = \frac{\delta_i^A - \delta_{min}^A}{\delta_{max}^A - \delta_{min}^A}$$
$$\mu_{o2}(\delta) = \frac{\delta_{max}^A - \delta_i^A}{\delta_{max}^A - \delta_{min}^A}. \quad (56)$$

Then, the gain of the proposed FDD law is obtainable using Eq. 53.

The performance of the proposed finite-time LPV-based FDD algorithm is compared with the finite-time LTI-based FDD law in Eq. 28.

3. *Scenario 3*: An experimental test, in this scenario, is carried out in indoor environment to further testify the effectiveness of the proposed FTC method. As shown in Fig. 3, this experimental platform consists of a UQH equipped with

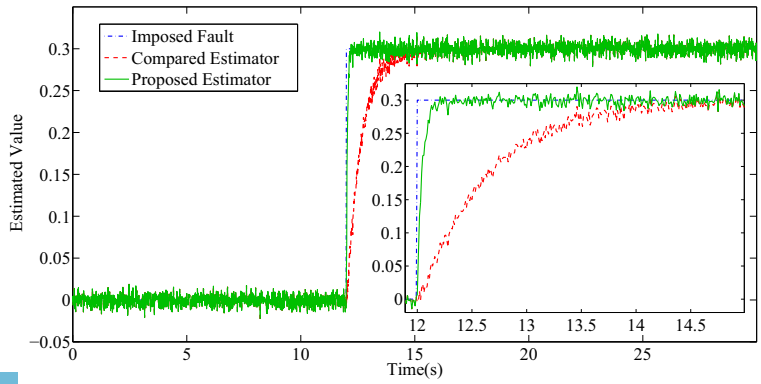

Fig. 10 Performance comparison of fault estimation

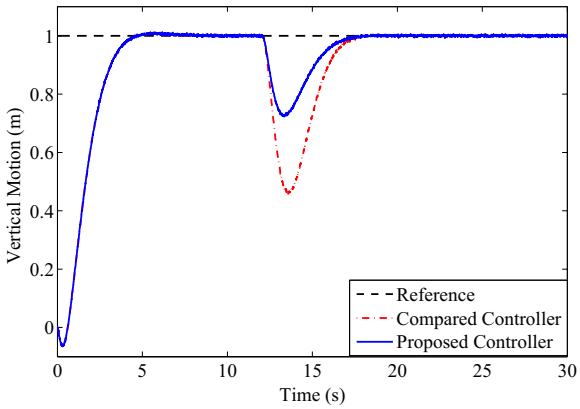

Fig. 11 Performance comparison in vertical direction

a Gumstix embedded computer hardware with operating software QuaRC (which is a convenient software developed by Quanser Inc. for the real-time implementation of algorithms developed in MATLAB/ Simulink environment to the practical vehicles), an object tracking system consisting of a network of 24 OptiTrack cameras (developed by NaturalPoint Inc.) is employed for providing the UQH's position and orientation since there is no GPS signals indoor, and a ground station for command distribution and data display in real-time.

A payload mass, approximately $0.2kg$, is mounted at the bottom of UQH. The voltage of battery decreases from $12.5V$ to $11.7V$, which indicates the control effectiveness drops from 100% to 80%. Both payload and battery voltage are assumed to be known in advance and changed at the beginning of experiment. Due to either the compared or the proposed controller is part of the full state-feedback control method, while

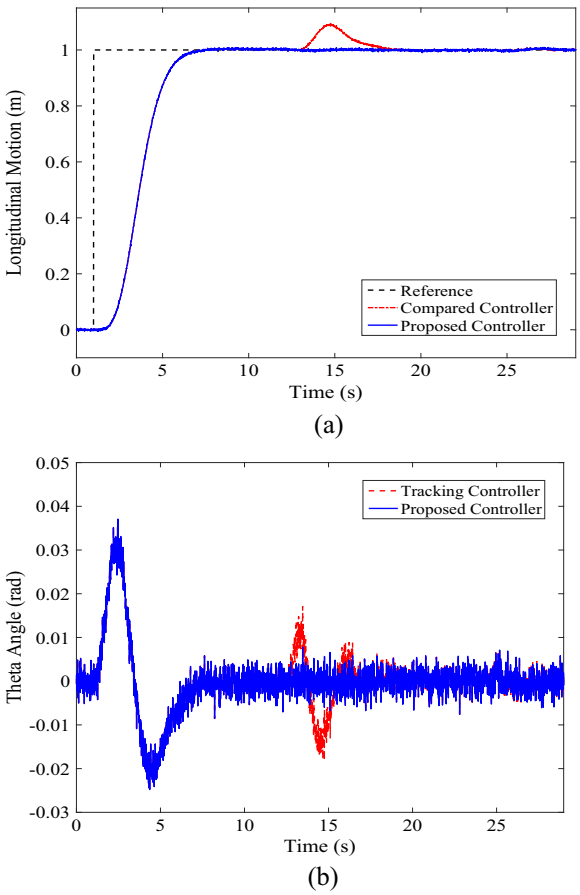

Fig. 12 Performance comparison in longitudinal direction (**a**) and pitch angles (**b**)

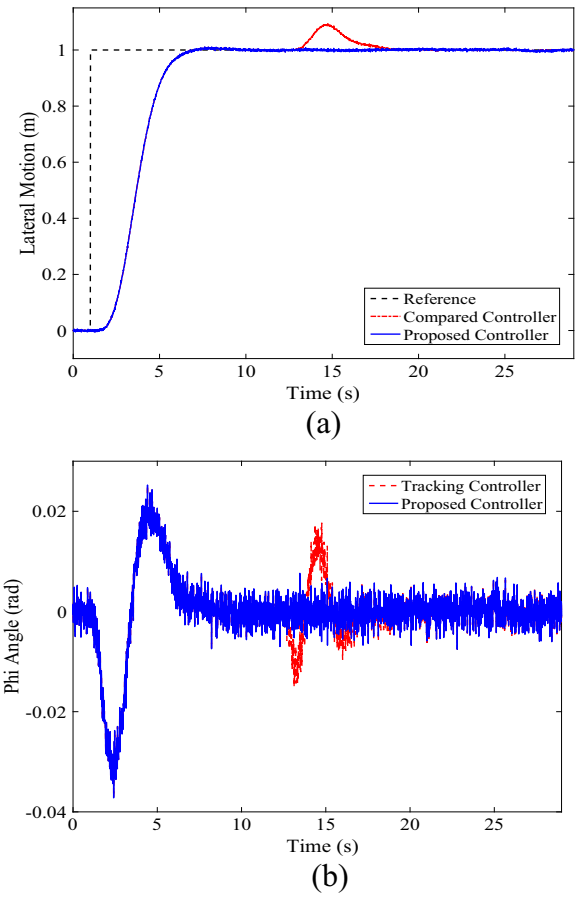

Fig. 13 Performance comparison in lateral direction (**a**) and roll angles (**b**)

the state of UQH, in practice, is partially measurable. Therefore, a classic Luenberger observer [49] and a low-pass filter (57) are used for estimating the state of UQH and filtering the noises from measurement.

$$\frac{x_{out}}{x_{in}} = \frac{30}{30+s}, \tag{57}$$

where x_{out}, x_{in}, and s are the output signal, input signal, and Laplace transform variable, respectively.

In addition, the weighting functions $\mu_{ci}(\delta)$ in this scenario are selected using the same rule Eq. 54 as in Scenario 2. $\delta^A_{max} = 1.8$, $\delta^B_{max} = 12.5$, $\delta^A_{min} = 1.4$ and $\delta^B_{min} = 11$.

Values of system parameters adopted for parameter estimation, control strategy design, as well as simulation validation are listed in Table 3. To avoid actuator saturation, control input (PWM signal) of each controller is constrained within [0, 0.05]. To demonstrate the proposed methods to be potential candidates toward practical applications, the noise, as an unavoidable phenomenon in practice, is imposed in the simulation as well. All measurement values of state are supposed to be polluted by Gaussian white noises, with 0.01 of sampling time and 0.0001 of covariance [1]. Furthermore, in the absence of actuator faults, the UQH is maneuvered by the baseline controller. 0.5s after the occurrence of faults, the proposed controller takes over the control of UQH.

4.2 Results and Performance Evaluation of Scenario 1

From Figs. 4 and 5, the estimation results of the two compared FDD schemes show that the proposed FDD scheme outperforms the compared one. The superior performance of the proposed scheme is attributed to the introduction of the additional sliding mode term $R(t)$ in Eq. 28, which tends to guarantee a fast parameter convergence in a specific time.

As displayed in Fig. 6, the proposed controller with less overshoot, in the presence of actuator fault, outperforms the compared controller. Figures 7a and 8a show that the system performance is considerably improved by the proposed controller with comparison of baseline controller in either longitudinal or lateral

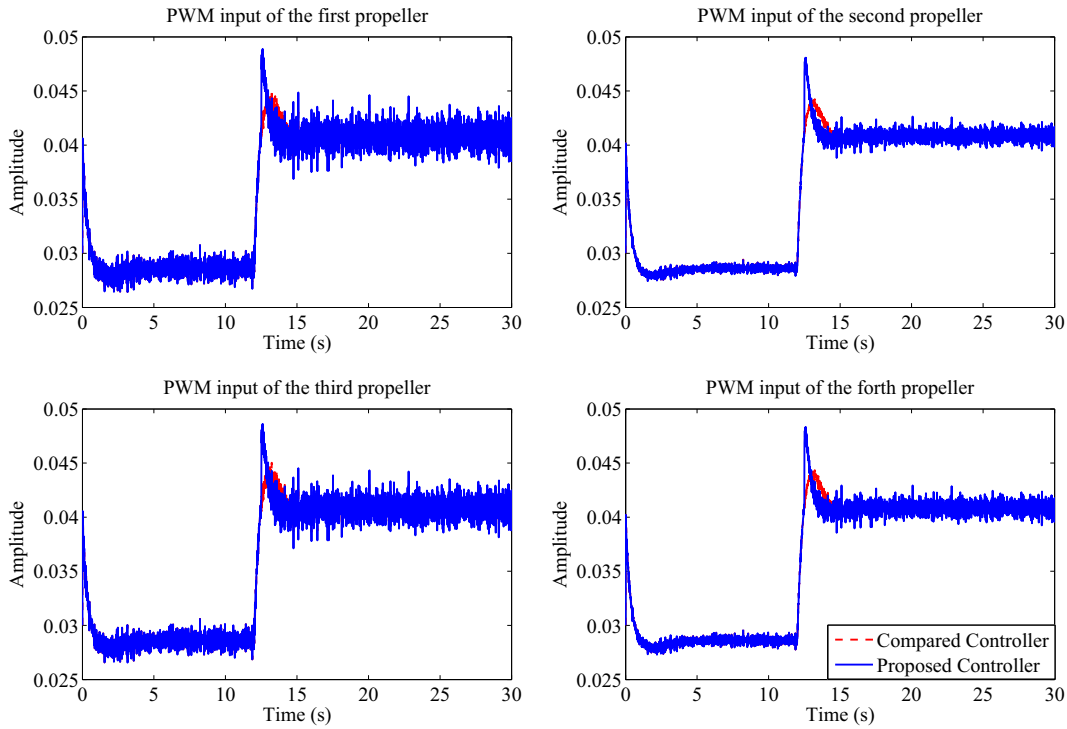

Fig. 14 Performance comparison of PWM signals

direction. The superior performance of the proposed controller, as shown in Figs. 7b and 8b, is due to the operation of UQH with more prompt angular action and less oscillation than the compared one.

From Fig. 9, comparing with the baseline controller, the proposed controller, which is subject to actuator saturation, can simultaneously regulate the thrust of UQH more prompt. This is exactly the cause of better performance of the proposed controller.

4.3 Results and Performance Evaluation of Scenario 2

Figure 10 shows that the proposed FDD method performs better than the compared one, although both of them contain the fast convergence term. This phenomenon is primarily caused by the LPV characteristic of the proposed scheme, which can adapt to the variation of payload, while the compared algorithm is constant despite the payload changes. Only the estimation result for the front motor is selected since its estimated value is similar to the rest three motors.

As revealed in Fig. 11, although the proposed and compared controllers are capable of operating the UQH back to the desired height after a transient period, the proposed controller can stabilize the system with less expense of overshoot than the baseline controller. From Figs. 12 and 13, better performance is also achieved by the proposed controller comparing with the baseline controller in either longitudinal or lateral direction.

Figure 14 displays that two compared controllers are all under actuator saturation, but the proposed controller can command actuators to operate as expected faster than the compared one, so as to properly mitigate the actuator faults with less time delay.

4.4 Results and Performance Evaluation of Scenario 3

Figure 15 shows that a residual of 0.1 m between the desired and real heights when the UQH is controlled by the compared controller, while the UQH tracks the reference height without obvious errors. The significant drop in altitude is due to the voltage loss in battery, while no corresponding compensation action is taken to the compared controller.

In addition, as seen in Fig. 16a, a significant deviation (around 0.6 m along the Y (lateral) direction is caused by the compared controller during the take-off period, while the proposed controller tracks the desired trajectory with relatively small error (around 0.12 m). Absence of mass variation counteracting

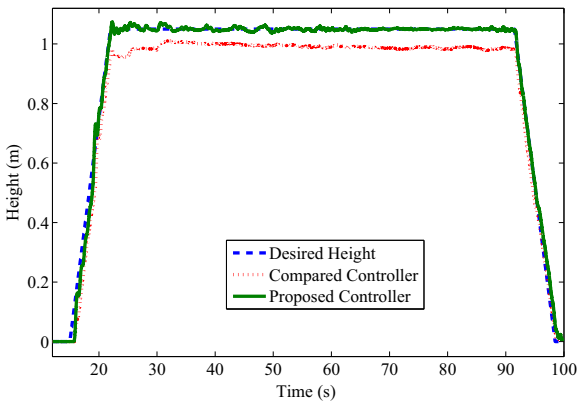

Fig. 15 Performance comparison in vertical direction

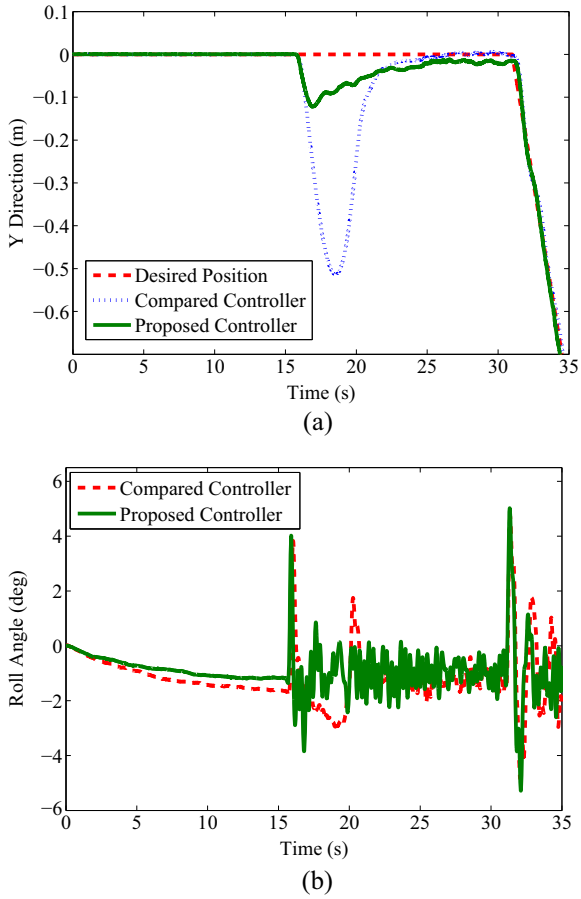

Fig. 16 Performance comparison in lateral direction (**a**) and the corresponding roll angles (**b**)

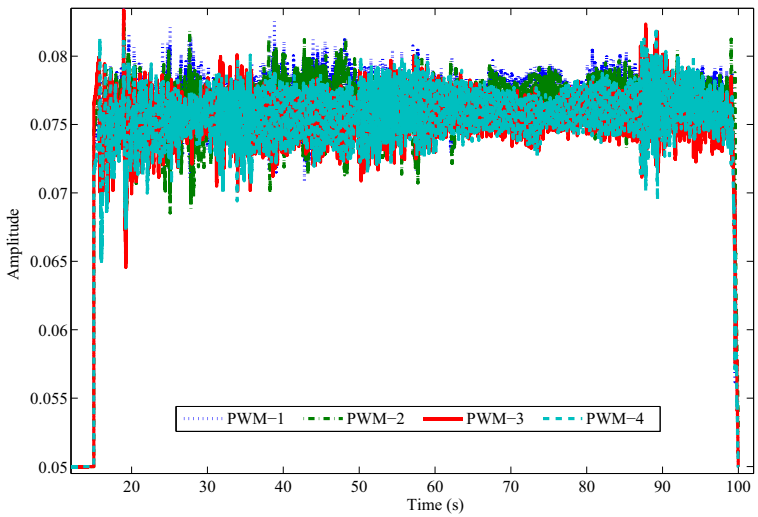

Fig. 17 PWM signals of the compared controller

mechanism in the compared controller results in its poor performance.

To be more specific, as the PWM signals of the two controllers recorded in Figs. 17 and 18, the proposed controller distributes control signals in apparent differences to the four motors, in contrast, the control signals of the compared controller assigned to distinct motors with almost identical values. This behavior is due to the fact that the control gains of the compared controller is fixed, and no PWM significantly varies when the system dynamic changes, which exactly explains the deterioration in its performance. Alternatively, owing to its reconfigurable properties, the proposed controller can correspondingly and effectively alter its PWM signals to counteract the adverse effects induced by the actuator faults and system dynamics variation.

5 Conclusion and Future Works

This paper presents a real-time fault detection, diagnosis, and tolerant control strategy for an unmanned quadrotor helicopter against actuator faults and system dynamics variations. The developed algorithm includes a linear parameter varying based parameter estimation and control strategy. The unmanned quadrotor helicopter is initially controlled by the baseline controller with healthy actuators and no dynamics variations. In the presence of actuator faults and

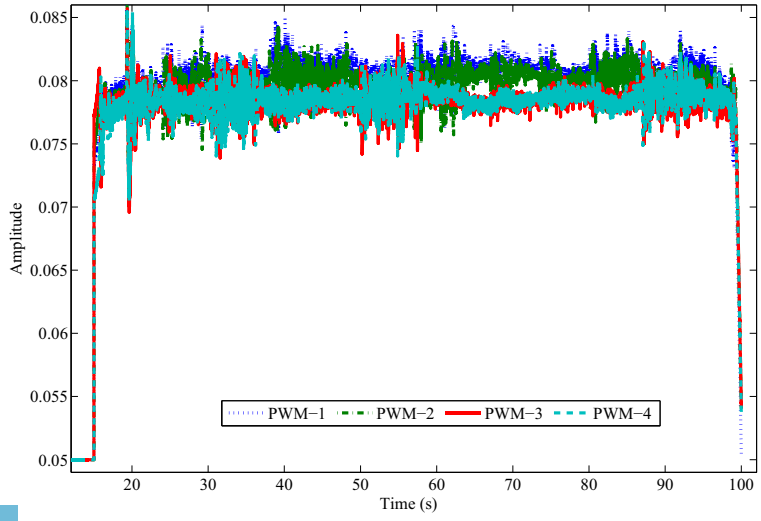

Fig. 18 PWM signals of the proposed controller

system dynamics variations, their values can be estimated first; the weighting functions are then calculated in real-time; the control gains, next, are readjusted according to the online obtained weighting functions; finally, the quadrotor helicopter is manipulated and stabilized by this regulated controller, intended to achieve the satisfactory performance. The results of simulation and experimental tests have convincingly proved that the proposed methodology is capable of satisfying the acceptable system performance demands in the absence/presence of payload variation and battery drainage.

Future works of this study may be extended to enhance the manoeuvrability of quadrotor helicopter by releasing the hovering hypothesis and including more time-varying system parameters. Furthermore, the uncertainties and nonlinearities in practical systems may cause the inefficacy and inaccuracy of model-based estimation law, more precise system identification is thereby suggested.

Acknowledgment The work reported in this paper is partially supported by NSERC, NNSFC #61573282, and SPNSF #2015JZ020.

References

1. Liu, Z.X., Yuan, C., Zhang, Y.M., Luo, J.: A learning-based fault tolerant tracking control of an unmanned quadrotor helicopter. J. Intell. Robot. Syst. **84**(1), 145–162 (2016)
2. Alexis, K., Nikolakopoulos, G., Tzes, A.: Switching model predictive attitude control for a quadrotor helicopter subject to atmospheric disturbances. Control. Eng. Pract. **19**(10), 1195–1207 (2011)
3. Zhang, Y.M., Chamseddine, A., Rabbath, C.A., Gordon, B.W., Su, C.Y., Rakheja, S., Fulford, C., Apkarian, J., Gosselin, P.: Development of advanced FDD and FTC techniques with application to an unmanned quadrotor helicopter testbed. J. Frankl. Inst. **350**(9), 2396–2422 (2013)
4. Castillo, P., Dzul, A., Lozano, R.: Real-time stabilization and tracking of a four-rotor mini rotorcraft. IEEE Trans. Control Syst. Technol. **12**(4), 510–516 (2004)
5. Dierks, T., Jagannathan, S.: Output feedback control of a quadrotor UAV using neural networks. IEEE Trans. Neural Netw. **21**(1), 50–66 (2010)
6. Shakernia, O., Ma, Y., Koo, T.J., Sastry, S.: Landing an unmanned air vehicle: Vision based motion estimation and nonlinear control. Asian J. Control **1**(3), 128–145 (1999)
7. Gomez-Balderas, J.E., Flores, G., Carrillo, L.G., Lozano, R.: Tracking a ground moving target with a quadrotor using switching control. J. Intell. Robot. Syst. **70**(1-4), 65–78 (2013)
8. Yuan, C., Zhang, Y.M., Liu, Z.X.: A survey on technologies for automatic forest fire monitoring, detection and fighting using UAVs and remote sensing techniques. Can. J. Forest Res. **45**(7), 783–792 (2015)
9. Guerrero, J.A., Garcia, P.C., Challal, Y.: Quadrotors formation control. J. Intell. Robot. Syst. **70**(1-4), 221–231 (2013)
10. Rinaldi, F., Chiesa, S., Quagliotti, F.: Linear quadratic control for quadrotors UAVs dynamics and formation flight. J. Intell. Robot. Syst. **70**(1-4), 203–220 (2013)
11. Saska, M., Krajník, T., Vonásek, V., Kasl, Z., Spurný, V., Přeučil, L.: Fault-tolerant formation driving mechanism designed for heterogeneous MAVs-UGVs groups. J. Intell. Robot. Syst. **73**(1-4), 603–622 (2014)
12. Mellinger, D., Michael, N., Kumar, V.: Trajectory generation and control for precise aggressive maneuvers with quadrotors. Int. J. Robot. Res. **0**(0), 1–11 (2012)
13. Escareño, J., Salazar, S., Romero, H., Lozano, R.: Trajectory control of a quadrotor subject to 2D wind disturbances. J. Intell. Robot. Syst. **70**(1-4), 51–63 (2013)
14. Mammarella, M., Campa, G., Napolitano, M.R., Fravolini, M.L., Gu, Y., Perhinschi, M.G.: Machine vision/GPS integration using EKF for the UAV aerial refueling problem. IEEE Trans. Syst. Man and Cybern. Part C (Appl. and Rev.) **38**(6), 791–801 (2008)
15. Bernard, M., Kondak, K., Maza, I., Ollero, A.: Autonomous transportation and deployment with aerial robots for search and rescue missions. J. Field Robot. **28**(6), 914–931 (2011)
16. Murphy, D.W., Cycon, J.: Applications for Mini VTOL UAV for Law Enforcement. Enabling Technologies for Law Enforcement and Security, International Society for Optics and Photonics, pp. 35–43 (1999)
17. Metni, N., Hamel, T.: A UAV for bridge inspection: Visual servoing control law with orientation limits. Autom. Constr. **17**(1), 3–10 (2007)
18. Pounds, P.E., Bersak, D.R., Dollar, A.M.: Stability of small-scale UAV helicopters and quadrotors with added payload mass under PID control. Auton. Robot. **33**(1-2), 129–142 (2012)
19. Annamalai, A.S.K., Sutton, R., Yang, C., Culverhouse, P., Sharma, S.: Robust adaptive control of an uninhabited surface vehicle. J. Intell. Robot. Syst. **78**(2), 319–338 (2015)
20. Sadeghzadeh, I., Abdolhosseini, M., Zhang, Y.M.: Payload drop application using an unmanned quadrotor helicopter based on gain-scheduled PID and model predictive control. Unmanned Syst. **2**(1), 39–52 (2014)
21. Wang, C., Nahon, M., Trentini, M.: Controller Development and Validation for a Small Quadrotor with Compensation for Model Variation. In: Proceedings of the International Conference on Unmanned Aircraft Systems (ICUAS), pp. 902–909 (2014)
22. Michael, N., Fink, J., Kumar, V.: Cooperative manipulation and transportation with aerial robots. Auton. Robot. **30**(1), 73–86 (2011)
23. Maza, I., Kondak, K., Bernard, M., Ollero, A.: Multi-UAV cooperation and control for load transportation and deployment. J. Intell. Robot. Syst. **57**(1-4), 417–449 (2010)
24. Zhang, Y.M., Jiang, J.: Bibliographical review on reconfigurable fault-tolerant control systems. Annu. Rev. Control. **32**(2), 229–252 (2008)

25. Efe, M.Ö.: Neural network assisted computationally simple $PI^{\lambda}d^{\mu}$ control of a quadrotor UAV. IEEE Trans. Ind. Inform. **7**(2), 354–361 (2011)
26. Efe, M.Ö.: Battery power loss compensated fractional order sliding mode control of a quadrotor UAV. Asian J. Control. **14**(2), 413–425 (2012)
27. Lai, L.C., Yang, C.C., Wu, C.J.: Time-optimal control of a hovering quad-rotor helicopter. J. Intell. Robot. Syst. **45**(2), 115–135 (2006)
28. Abdolhosseini, M., Zhang, Y.M., Rabbath, C.A.: An efficient model predictive control scheme for an unmanned quadrotor helicopter. J. Intell. Robot. Syst. **70**(1-4), 27–38 (2013)
29. Shamma, J.S.: An Overview of LPV Systems. In: Control of Linear Parameter Varying Systems with Applications. Springer, US (2011)
30. Hoffmann, C., Werner, H.: A survey of linear parameter-varying control applications validated by experiments or high-fidelity simulations. IEEE Trans. Control Syst. Technol. **23**(2), 416–433 (2015)
31. Wu, F., Dong, K.: Gain-scheduling control of LFT systems using parameter-dependent Lyapunov functions. Automatica **42**(1), 39–50 (2006)
32. Shamma, J.S.: Analysis and design of gain scheduled control systems. Doctoral dissertation Massachusetts Institute of Technology (1988)
33. Wu, F.: A generalized LPV system analysis and control synthesis framework. Int. J. Control. **74**(7), 745–759 (2001)
34. Blanchini, F., Miani, S.: Set-theoretic methods in control Springer (2008)
35. Blanchini, F., Casagrande, D., Miani, S., Viaro, U.: Stable LPV realization of parametric transfer functions and its application to gain-scheduling control design. IEEE Trans. Autom. Control. **55**(10), 2271–2281 (2010)
36. Zhang, Y.M., Jiang, J.: Fault tolerant control system design with explicit consideration of performance degradation. IEEE Trans. Aerosp. Electron. Syst. **39**(3), 838–848 (2003)
37. Zhang, Y.M., Jiang, J.: Active fault-tolerant control system against partial actuator failures. IEE Control Theory and Appl. **149**(1), 95–104 (2002)
38. Rotondo, D., Nejjari, F., Puig, V.: Robust quasi-LPV model reference FTC of a quadrotor UAV subject to actuator faults. Int. J. Appl. Math. Comput. Sci. **25**(1), 7–22 (2015)
39. Amoozgar, M.H., Chamseddine, A., Zhang, Y.M.: Experimental test of a two-stage Kalman filter for actuator fault detection and diagnosis of an unmanned quadrotor helicopter. J. Intell. Robot. Syst. **70**(1-4), 107–117 (2013)
40. Apkarian, P., Gahinet, P., Becker, G.: Self-scheduled $h\infty$ control of linear parameter-varying systems: A design example. Automatica **31**(9), 1251–1261 (1995)
41. Stevens, B.L., Lewis, F.L.: Aircraft control and simulation John Wiley & Sons (2003)
42. Heemels, W.H., Daafouz, J., Millerioux, G.: Observer-based control of discrete-time LPV systems with uncertain parameters. IEEE Trans. Autom. Control. **55**(9), 2130–2135 (2010)
43. Stilwell, D.J., Rugh, W.J.: Interpolation of observer state feedback controllers for gain scheduling. IEEE Trans. Autom. Control. **44**(6), 1225–1229 (1999)
44. Bhat, S.P., Bernstein, D.S.: Continuous finite-time stabilization of the translational and rotational double integrators. IEEE Trans. Autom. Control. **43**(5), 678–682 (1998)
45. Boyd, S.P., El Ghaoui, L., Feron, E., Balakrishnan, V.: Linear matrix inequalities in system and control theory Philadelphia: Society for Industrial and Applied Mathematics (1994)
46. Yu, X., Jiang, J.: Hybrid fault-tolerant flight control system design against partial actuator failures. IEEE Trans. Control Syst. Technol. **20**(4), 871–886 (2012)
47. Apkarian, P., Adams, R.J.: Advanced gain-scheduling techniques for uncertain systems. IEEE Trans. Control Syst. Technol. **6**(1), 21–32 (1998)
48. Montes de Oca, S., Tornil-Sin, S., Puig, V., Theilliol, D.: Fault-tolerant control design using the linear parameter varying approach. Int. J. Robust Nonlinear Control **24**(14), 1969–1988 (2014)
49. Khalil, H.K., Grizzle, J.W.: Nonlinear Systems. Prentice Hall, New Jersey (1996)

Zhixiang Liu is currently doing post-doctoral research in Loria at University of Lorraine, Nancy, France. He did his Ph.D. research in the Department of Mechanical and Industrial Engineering at Concordia University, Montreal, QC, Canada. His research interests include fault detection, diagnosis and tolerant control of safety-critical systems, collision avoidance, robotic systems design, as well as guidance, navigation, and control of unmanned aerial/ground/surface vehicles.

Chi Yuan is currently a Ph.D. candidate in mechanical engineering with the Department of Mechanical and Industrial Engineering at Concordia University, Montreal, QC, Canada. Her research interests include unmanned aerial/ground vehicles-based forest fire monitoring, detection and fighting, visual and infrared image processing, data fusion, intelligent decision making, and vision-based robotic navigation.

Youmin Zhang received the B.S., M.S., and Ph.D. degrees from Northwestern Polytechnical University, Xi'an, China, in 1983, 1986, and 1995, respectively. He is currently a Professor with the Department of Mechanical and Industrial Engineering and the Concordia Institute of Aerospace Design and Innovation, Faculty of Engineering and Computer Science, Concordia University, Montreal, Quebec, Canada. His current research interests include condition monitoring, health management, fault diagnosis, and fault-tolerant (flight) control systems; cooperative guidance, navigation, and control (GNC) and remote sensing of single and multiple unmanned aerial/space/ground/surface vehicles and their applications to monitoring, detection and services missions for forest fires, powerlines and pipelines, as well as search and rescue; dynamic systems modeling, estimation, identification, advanced control and signal processing techniques for diagnosis, prognosis, and health management of safety-critical systems, renewable energy systems and smart grids, as well as manufacturing processes. He has authored four books, over 420 journal and conference papers, and book chapters. He is a Senior Member of the American Institute of Aeronautics and Astronautics (AIAA) and the Institute of Electrical and Electronics Engineers (IEEE), and a member of the Technical Committee (TC) for several scientific societies, including the International Federation of Automatic Control TC on Fault Detection, Supervision and Safety for Technical Processes, the AIAA Infotech@Aerospace Program Committee on Unmanned Systems, the IEEE Robotics and Automation Society TC on Aerial Robotics and Unmanned Aerial Vehicles, the ASME/IEEE TC on Mechatronics and Embedded Systems and Applications, and the International Conference on Unmanned Aircraft Systems (ICUAS) Association Executive Committee. He has been invited to deliver plenary talks at international conferences/workshops and research seminars worldwide for over 80 times. He is an Editor-in-Chief of the Journal of Instrumentation, Automation and Systems, an Editor-at-Large of the Journal of Intelligent & Robotic Systems, and an Editorial Board Member/Associate Editor of several other international journals (including three newly launched journals on Unmanned Systems). He has served as General Chair, Program Chair, and IPC Member of many international conferences, including the General Chair of the 10th International Conference on Intelligent Unmanned Systems (ICIUS) in 2014, Montreal, Canada, Program Chair of the International Conference on Unmanned Aircraft Systems (ICUAS) in 2014, Orlando, FL, USA, one of General Chairs of the ICUAS in 2015, Denver, USA, a Co-General Chair of the ICIUS 2016 held at Xian, China, and Program Chair of the ICUAS 2017 to be held at Miami, USA. More detailed information can be found at http://users.encs.concordia.ca/~ymzhang/index.html.